Phosphorylation of KIN-G motor domain by Polo-like kinase negatively regulates centrin arm biogenesis in *Trypanosoma brucei*

Yasuhiro Kurasawa[1,§], Qing Zhou[1,§], Kyu Joon Lee[2,§], Huiqing Hu[1], and Ziyin Li[1,*]

[1]Department of Microbiology and Molecular Genetics, McGovern Medical School, University of Texas Health Science Center at Houston, Houston, TX 77030

[2]Department of Tropical Medicine, College of Medicine, Soon Chun Hyang University, South Korea

[§]These authors contributed equally to this work.

*To whom correspondence should be addressed. Tel: 1-713-500-5139; Fax: 1-713-500-5499; E-mail: Ziyin.Li@uth.tmc.edu

Running title: TbPLK negatively regulates KIN-G

Abstract

The unicellular parasite *Trypanosoma brucei* assembles a motile flagellum that is required for locomotion, cell division plane placement, and cell-cell communication. Inheritance of the flagellum during the cell cycle relies on the faithful duplication/segregation of multiple flagellum-associated cytoskeletal structures, including a centrin-marked, bar-shaped structure termed centrin arm, which also determines the biogenesis site for Golgi. Biogenesis of the centrin arm requires the Polo-like kinase homolog TbPLK and the orphan kinesin KIN-G, but whether TbPLK regulates KIN-G is unclear. Here we report that TbPLK phosphorylates KIN-G, disrupts its microtubule-binding activity, and negatively regulates its function in the procyclic form of *T. brucei*. TbPLK phosphorylates KIN-G *in vitro* at multiple residues, some of which are phosphorylated *in vivo* in *T. brucei*, including the Thr301 residue within one of the microtubule-binding motifs of the kinesin motor domain. Phosphorylation of Thr301 by TbPLK inhibits the microtubule-binding activity of KIN-G *in vitro*, and expression of a Thr301 phospho-mimic mutant in *T. brucei* disrupts centrin arm integrity, thereby impairing Golgi biogenesis, flagellum attachment zone elongation, flagellum positioning, and cell division plane placement. Therefore, TbPLK negatively regulates KIN-G activity by phosphorylating Thr301, and dephosphorylation of Thr301 is required for KIN-G to fulfill its cellular function in promoting centrin arm biogenesis.

Importance

Trypanosoma brucei is an early branching protozoan, which causes sleeping sickness in humans and nagana in cattle in sub-Saharan Africa. This parasite possesses a motile flagellum to control motility, morphogenesis, and proliferation, and inheritance of the flagellum during the cell cycle depends on a specialized flagellum-associated cytoskeletal structure termed the centrin arm. Biogenesis of the centrin arm requires the evolutionarily conserved Polo-like kinase homolog TbPLK and a trypanosome-specific orphan kinesin named KIN-G. In trypanosome cells KIN-G is phosphorylated, but it was unclear whether KIN-G is a substrate of TbPLK and whether phosphorylation of KIN-G regulates its function. In this report, we demonstrated that TbPLK phosphorylated KIN-G *in vitro* at multiple sites, including the Thr301 residue located within one of the three microtubule-binding motifs of the kinesin motor domain, which was previously reported as an *in vivo* phosphosite in trypanosome cells. We further showed that TbPLK inhibited the microtubule-binding activity of KIN-G and that phosphorylation of Thr301 disrupted the microtubule binding activity of KIN-G and the cellular function of KIN-G by impairing centrin arm biogenesis, which further impairing FAZ elongation, flagellum segregation, cell division plane placement, and Golgi biogenesis. These findings uncover a negative regulation of KIN-G activity by TbPLK-mediated phosphorylation of Thr301 in the kinesin motor domain.

Introduction

The early branching parasitic protozoan *Trypanosoma brucei* causes sleeping sickness in humans and nagana in cattle in sub-Saharan Africa, and it possesses a single flagellum, which is required for cell motility, cell division, and cell-cell communication. The flagellum originates from the basal body, which has a typical structure of centrioles in eukaryotes, exits the cell body through the flagellar pocket, and extends toward the anterior tip of the cell by attaching to the cell membrane via the flagellum attachment zone (FAZ), a specialized cytoskeletal structure consisting of the intra-cellular FAZ filament, the flagellum FAZ domain, and the junction between the flagellar membrane and the cell membrane (1). At the proximal end of the flagellum and near the flagellar pocket region, there sit several flagellum-associated cytoskeletal structures, including the flagellar pocket collar (FPC) (2) and the hook complex (3). The horseshoe-shaped FPC, which is marked by TbBILBO1, wraps around the flagellum, whereas the hairpin-shaped hook complex, which consists of a fishhook-like structure marked by TbMORN1 and a bar-shaped structure named centrin arm and marked by TbCentrin2 (3, 4), sits on the top of the FPC (3). Between the mature basal body and the pro-basal body, there originates a specialized set of four microtubules termed the microtubule quartet (MtQ), which passes through the hook complex and the FPC and extends, alongside the intracellular FAZ filament, to the anterior tip of the cell (3, 5). The intracellular FAZ filament originates from a region within the hook complex structure (3) and elongates alongside the MtQ toward the anterior cell tip (6, 7). In close proximity to the centrin arm, the Golgi apparatus is located (8), and it sits next to the endoplasmic reticulum exit site (ERES), thereby forming unique junctions to facilitate protein trafficking (9).

During the S phase of the cell cycle in *T. brucei*, a new pair of mature basal body/pro-basal body is assembled, followed by the assembly of a new flagellum from the mature basal body and the subsequent assembly of the flagellum-associated cytoskeletal structures. The newly synthesized flagellum and its associated, newly synthesized cytoskeletal structures are segregated into the new-flagellum daughter (NFD) cell, whereas the old-flagellum daughter (OFD) cell inherits the existing flagellum and its associated cytoskeletal structures (10). Segregation or positioning of the newly assembled flagellum depends on the faithful duplication and segregation of its associated cytoskeletal structures, which further impacts the placement of the cell division plane/cleavage furrow and the faithful division of the daughter cells (11-14). During the cell cycle, the Golgi apparatus undergoes *de novo* duplication, assembling a new Golgi next to the old Golgi in a centrin arm-dependent manner (15), and the newly assembled Golgi is segregated into the NFD cell, likely by associating with the newly assembled centrin arm through the scaffold protein CAAP1 (16).

The precise functions of the hook complex remain elusive, but its deficiency often leads to defects in the elongation of the new FAZ filament, the positioning of the new flagellum, the placement of cell division plane, and, consequently, cytokinesis (11, 12, 16-18). Several regulatory proteins that control hook complex biogenesis/assembly have been identified, including the Polo-like kinase homolog TbPLK (19), the kinetoplastid-specific protein phosphatase KPP1 (20), the E3 ubiquitin ligase complex $CRL4^{WDR1}$ (21), the orphan kinesin KIN-G (16), and the KIN-G-interacting protein WDR2 (18). TbPLK phosphorylates the centrin

arm protein TbCentrin2 to promote centrin arm duplication (22), whereas its protein abundance is regulated by $CRL4^{WDR1}$, thereby impacting centrin arm biogenesis (21). KIN-G is a microtubule plus end-directed motor protein, which localizes to centrin arm and regulates centrin arm biogenesis (16), and WDR2 promotes centrin arm biogenesis by recruiting KIN-G (18). KIN-G is phosphorylated at multiple residues *in vivo* in trypanosome cells (18, 23), but the protein kinase responsive for KIN-G phosphorylation was not identified previously, and whether phosphorylation of KIN-G may regulate KIN-G function remains unknown.

Here we report that TbPLK phosphorylates KIN-G at multiple sites, including the Thr301 residue in one of the microtubule-binding motifs of the motor domain, and that phosphorylation of Thr301 inhibits the microtubule-binding activity of KIN-G. We further show that phosphorylation of Thr301 disrupts the cellular function of KIN-G by impairing centrin arm biogenesis, which further impacts FAZ elongation, flagellum positioning, cell division plane placement, and Golgi biogenesis. These results suggest that TbPLK negatively regulates KIN-G activity through phosphorylating Thr301 and that dephosphorylation of Thr301 is required for KIN-G to exert its cellular function in the procyclic form of *T. brucei*. This finding underscores a novel control mechanism of KIN-G by the Polo-like kinase in regulating centrin arm biogenesis in *T. brucei*.

Results

TbPLK co-localizes with KIN-G at centrin arm and phosphorylates KIN-G *in vitro*

The findings that TbPLK and KIN-G are both required for the biogenesis of the centrin arm and its associated Golgi apparatus (16, 19) and that KIN-G is phosphorylated *in vivo* in trypanosome cells (18, 23) prompted us to test whether TbPLK may phosphorylate KIN-G and thus may regulate KIN-G function. We first investigated when the two proteins may co-localize during the cell cycle by co-immunofluorescence microscopy analysis of cells expressing endogenously triple HA-tagged KIN-G. During G1 phase, TbPLK and KIN-G co-localized at the centrin arm, with KIN-G more enriched at the distal end of the centrin arm (Fig. 1A). During early S-phase when the centrin arm started to duplicate, KIN-G and TbPLK co-localized, almost entirely, to the elongating centrin arm (Fig. 1A, S-phase cell on the left). When cells gradually progressed to late S-phase, the centrin arm was further elongated and finally separated to two structures, KIN-G localized to the elongating centrin arm (Fig. 1A, S-phase cell in the middle) and the separated centrin arm structures, respectively (Fig. 1A, S-phase cell on the right). However, during these stages, TbPLK was enriched at the new FAZ tip and the flagella connector, with a small amount of TbPLK remaining on the old centrin arm, where it co-localized with KIN-G (Fig. 1A, S-phase cells in the middle and on the right). During G2 phase when the two centrin arms were farther separated, KIN-G remained on the two centrin arm structures, but TbPLK no longer resided on the centrin arm, but was enriched on the new FAZ tip and the flagella connector (Fig. 1A). Note that from G1 phase to G2 phase, TbPLK additionally localized to the basal body (Fig. 1A).

We asked whether TbPLK may phosphorylate KIN-G, so we performed *in vitro* kinase assay using purified recombinant TbPLK and KIN-G proteins and ATP-γ-S for thio-phosphorylation and subsequent detection of

thio-phosphorylated proteins by the anti-PNBM antibody (24). We detected auto-phosphorylation of TbPLK, indicating active TbPLK, and phosphorylation of KIN-G (Fig. 1B), suggesting that KIN-G is an *in vitro* substrate for TbPLK. To identify the *in vitro* TbPLK phosphosites on KIN-G, we performed *in vitro* kinase assay with purified recombinant TbPLK and KIN-G proteins and regular ATP, and then separated the proteins by SDS-PAGE, which showed that the phosphorylated KIN-G protein migrated slower than the non-phosphorylated KIN-G protein (Fig. 1C). The phosphorylated KIN-G protein band was excised and analyzed by mass spectrometry, which identified 29 *in vitro* TbPLK phosphosites (Fig. 1D), among which 10 sites have been previously identified as *in vivo* phosphosites (18, 23). Five out of these 10 phosphosites, Thr32, Thr72, Ser194, and Thr301, are located within the motor domain of KIN-G, with Thr301 located in the microtubule-binding motif #3 (Fig. 1D, E). The remaining five sites, Thr388, Thr523, Ser553, Ser556, and Thr617, are located in the C-terminal coiled-coil motifs and in the loop between coiled-coil motifs #2 and #3 (Fig. 1D). The identification of ten *in vitro* TbPLK phosphosites that are also phosphorylated *in vivo* in trypanosome cells suggests that these sites could be potential *in vivo* TbPLK phosphosites.

TbPLK phosphorylation of KIN-G disrupts KIN-G binding to microtubules

Because TbPLK co-localized with KIN-G during early cell cycle stages at the centrin arm and phosphorylates KIN-G in the microtubule-binding motif (Fig. 1), we tested the effect of TbPLK phosphorylation on the microtubule-binding activity and/or microtubule-gliding activity of KIN-G by *in vitro* microtubule-binding and -gliding assay (16). Purified recombinant KIN-G protein was first settled onto glass coverslips in a flow chamber, and then rhodamine-labeled microtubules were added into the flow chamber, where microtubules first bound to KIN-G and then moved toward their minus-ends (opposite to the plus end-directed moving direction of KIN-G) (16). We detected strong binding of microtubules when only KIN-G was settled on the coverslips or together with the kinase-dead TbPLK mutant $TbPLK^{K70R}$, but we observed a significant reduction in the number of attached microtubules when TbPLK was co-settled with KIN-G (Fig. 2A, B), suggesting that TbPLK activity inhibits the microtubule-binding activity of KIN-G. In the presence of $TbPLK^{K70R}$, the microtubule gliding speed of KIN-G was slightly, but insignificantly, reduced (Fig. 2C), which suggests that the binding of $TbPLK^{K70R}$ to KIN-G somewhat interfered with its motility on microtubules.

We next performed *in vitro* microtubule-binding and -gliding assay by adding TbPLK after incubating microtubules with settled KIN-G on the glass coverslip (Fig. 2D). Without adding TbPLK, the number of bound microtubules decreased by an average of ~30% at 12 min, whereas when TbPLK was added into the chamber, the number of bound microtubules decreased by an average of ~83% at 12 min (Fig. 2D, E), demonstrating that TbPLK-mediated phosphorylation caused the detachment of the microtubules that had attached to KIN-G before the addition of TbPLK. Together, these results suggest that the kinase activity of TbPLK inhibits the binding of KIN-G to microtubules.

Phosphorylation of Thr301 in KIN-G by TbPLK impairs the binding of KIN-G to microtubules

Because TbPLK phosphorylates the Thr301 residue within the microtubule-binding motif #3 of KIN-G (Fig. 1) and TbPLK disrupts the microtubule-binding activity of KIN-G *in vitro* (Fig. 2), we asked whether phosphorylation of Thr301 may disrupt the microtubule-binding activity *in vitro*. We mutated Thr301 to generate phospho-mimic and phospho-deficient mutants, KIN-G^{T301D} and KIN-G^{T301A}, respectively, purified the recombinant proteins, and used them in the *in vitro* microtubule-binding and -gliding assay. The results showed that KIN-G^{T301A} had similar microtubule-binding activity to wild-type KIN-G, but KIN-G^{T301D} lost microtubule-binding activity (Fig. 3A, B), demonstrating that phosphorylation of Thr301 by TbPLK disrupted the microtubule-binding activity. Notably, the microtubule-gliding activity of KIN-G^{T301A} was moderately, but insignificantly, reduced (Fig. 3C), suggesting that mutation of this residue somehow reduced the motility of KIN-G, although the reduction in motility does not affect the cellular function of KIN-G^{T301A} (see below).

We also mutated the Thr284 residue, an *in vitro* TbPLK phosphosite located in the microtubule-binding motif #2 (Fig. 1E), to generate phospho-mimic and phospho-deficient mutants, KIN-G^{T284D} and KIN-G^{T284A}, respectively, and tested their microtubule-binding and -gliding activity. Neither KIN-G^{T284D} nor KIN-G^{T284A} showed any defects in microtubule-binding and -gliding activity (Fig. 3).

Phosphorylation of Thr301 in KIN-G by TbPLK causes defective cell proliferation

We ectopically expressed triple HA-tagged KIN-G^{T301D}, KIN-G^{T301A}, and KIN-G, which were recoded to resist RNAi, in the KIN-G RNAi cell line to investigate the potential effects on the cellular function of KIN-G in the procyclic form of *T. brucei*. Immunofluorescence microscopy showed that like wild-type KIN-G, both KIN-G mutants were localized to the centrin arm (Fig. 4A), suggesting that phosphorylation of KIN-G does not affect its subcellular localization. Western blotting confirmed the knockdown of endogenously PTP-tagged KIN-G and the ectopic expression of triple HA-tagged wild-type and mutant KIN-G (Fig. 4B). Expression of wild-type KIN-G and KIN-G^{T301A}, but not KIN-G^{T301D}, both rescued the growth defects of KIN-G RNAi cells (Fig. 4C). We further quantitated the cell types of different nucleus and kinetoplast configurations in KIN-G RNAi cells and the three complementation cells. The KIN-G^{T301D} complementation cells, but not the KIN-G complementation cells and the KIN-G^{T301A} complementation cells, accumulated 2N1K (two nuclei and one kinetoplast) cells and xNyK ($x>2$; $y\geq1$) cells, similar to the phenotype caused by KIN-G RNAi (Fig. 4D). These results suggest that Thr301 phosphorylation disrupted the cellular function of KIN-G in trypanosomes.

Phosphorylation of Thr301 in KIN-G disrupts centrin arm and Golgi biogenesis

The potential effect of Thr301 phosphorylation on the function of KIN-G in centrin arm biogenesis was examined by immunofluorescence microscopy using anti-TbCentrin4 and the pan-centrin antibody 20H5. Measurement of the length of the new and old centrin arm structures showed that many KIN-G^{T301D} complementation cells contained a shorter new centrin arm, with the average length of the new centrin arm significantly reduced after tetracycline induction for 48 h (Fig. 5A, B). The results mimicked the deficiency in

the biogenesis of the new centrin arm in KIN-G RNAi cells (16), suggesting that phosphorylation of Thr301 in KIN-G disrupted its function in promoting centrin arm biogenesis.

The potential effect of Thr301 phosphorylation on Golgi biogenesis was also investigated by immunofluorescence microscopy using the anti-TbGRASP antibody. We endogenously epitope-tagged the COPII coat protein subunit Sec13 with mCherry to serve as a marker for the ER exit site (ERES). In non-induced control, two major Golgi/ERES (strong TbGRASP/Sec13 fluorescence signal) were detected in bi-nucleated cells, and one or two smaller Golgi (weaker TbGRASP signal), each of which associated with a smaller ERES (weaker Sec13 signal), were also detected near the major Golgi/ERES in some bi-nucleated cells (Fig. 5C, open arrows and solid arrowheads, respectively). In KIN-G^{T301D} complementation cells, the number of bi-nucleated cells containing two, three, or four Golgi/ERES were significantly reduced, whereas the number of bi-nucleated cells containing more than four Golgi/ERES were significantly increased (Fig. 5C, D). These results suggest that phosphorylation of Thr301 in KIN-G disrupted its function in promoting Golgi biogenesis.

Phosphorylation of Thr301 in KIN-G impairs FAZ elongation and flagellum positioning

We investigated the potential effect of Thr301 phosphorylation on the elongation of the new FAZ by immunofluorescence microscopy using the anti-CC2D antibody (14), which showed that the length of the new FAZ in the bi-nucleated KIN-G^{T301D} complementation cells was significantly shorter than that of the non-induced bi-nucleated cells (Fig. 6A, B), suggesting that Thr301 phosphorylation impairs FAZ elongation. Notably, in these bi-nucleated KIN-G^{T301D} complementation cells, the size of the NFD cell was also smaller, which is positively correlated to the length of the new FAZ (Fig. 6C), in agreement with the finding that the FAZ length determines the cell size in trypanosomes (14), acting as the “cellular ruler” of trypanosome cell morphology (1).

The formation of a shorter new FAZ in KIN-G^{T301D} complementation cells prompted us to examine the segregation of the flagellum-associated cytoskeletal structures. Co-immunofluorescence microscopy with YL1/2, which labels the mature basal body (25), and anti-TbBILBO1 antibody, which labels the flagellar pocket collar (26), showed that in the bi-nucleated KIN-G^{T301D} complementation cells the duplicated basal bodies/flagellar pocket collars were not far segregated (Fig. 6D), with the average distance between the duplicated structures reduced significantly after tetracycline induction for 48 h (Fig. 6E, F). These results suggest that phosphorylation of Thr301 inhibits the segregation of flagellum-associated cytoskeletal structures. As the flagellum is nucleated from the mature basal body, these results suggest that Thr301 phosphorylation inhibits flagellum positioning.

Phosphorylation of Thr301 in KIN-G causes mis-placement of the cell division plane

Knockdown of KIN-G by RNAi caused cytokinesis defects (16), likely due to the mis-placement of the cell division plane, but this phenotype was not explored previously. Therefore, we investigated the potential defect in cell division plane placement in KIN-G RNAi cells by analyzing the localization of the orphan kinesin protein

KLIF, which marks the cell division plane during cytokinesis in trypanosomes (27). In the non-induced control cells, the leading edge of the KLIF-labeled cell division plane was always placed at the mid-portion of the ventral side of the NFD cell (Fig. 7A, yellow arrow). In contrast, in the dividing KIN-G RNAi cells, the leading edge of the KLIF-labeled cell division plane was placed in close proximity to the posterior cell tip (Fig. 7A, yellow arrows). We further investigated the effect of KIN-G RNAi on the positioning of the nascent posterior of the OFD cell, which is formed near the mid-portion of the ventral edge of the NFD cell through microtubule bundling and cytoskeleton remodeling (28). We used the epitope-tagged GB4 protein (Fig. 7B), a microtubule plus end-localized protein (29), as a marker for the cell posterior, and performed immunofluorescence microscopy. In control cells, the GB4-labeled nascent posterior was located at the mid-portion of the ventral side of the NFD cell, whereas in KIN-G RNAi cells, the GB4-labeled nascent posterior was placed next to the GB4-labeled existing posterior (Fig. 7B), which was confirmed by measurement of the inter-posterior distance (Fig. 7C).

The KIN-G^{T301D} complementation cells also appear to have cytokinesis defects (Fig. 4C, D). The number of bi-nucleated cells undergoing cytokinesis or with a visible cleavage furrow was significantly increased upon tetracycline induction (Fig. 7D, E), suggesting that the KIN-G^{T301D} complementation cells initiated cytokinesis, but failed to complete cytokinesis. Notably, those cells with a visible cleavage furrow appeared to contain a mis-placed cell division plane in the KIN-G^{T301D} complementation cells (Fig. 7D, yellow arrows). The mis-placement of the cell division plane was more prominent in the bi-nucleated cells with the NKKN configuration and the NKN configuration, in which the duplicated kinetoplasts were only partly separated or not separated, respectively, than in the bi-nucleated cells with the KNKN configuration (Fig. 7F). Therefore, phosphorylation of Thr301 in KIN-G disrupted cell division plane placement, mimicking the defect caused by KIN-G RNAi.

Discussion

In this report, we have identified the orphan kinesin KIN-G as a substrate of TbPLK, one of the two Polo-like kinase homologs in *T. brucei* (30), and discovered a negative role of TbPLK phosphorylation in regulating the biochemical activity and cellular function of KIN-G in the procyclic form of *T. brucei*. TbPLK is known to play multiple roles in basal body rotation, centrin arm assembly, FAZ elongation, cytokinesis, and Golgi biogenesis (19, 22, 31-35), but the mechanistic roles of TbPLK in regulating these cellular processes have not been fully elucidated, mainly because most of its substrates have not been identified. TbPLK phosphorylates the basal body-localized protein SPBB1 (13), the centrin arm protein TbCentrin2 (19, 22), and the cytokinesis regulators CIF1 and CIF2 (36), which exemplifies its role in regulating the rotation/segregation of basal body, the biogenesis of centrin arm and Golgi, and the initiation of cytokinesis, respectively. Phosphorylation of TbCentrin2 by TbPLK at Ser54 does not appear to be essential, as expression of the Ser54 phospho-deficient mutant TbCentrin2^{S54A} caused weak growth defects, whereas expression of the Ser54 phospho-mimic mutant TbCentrin2^{S54D} caused severe growth defects, suggesting that the dephosphorylation of TbCentrin2 at Ser54 is required for TbCentrin2 to execute its function in centrin arm assembly (22). However, it remains unclear how

phosphorylation of Ser54 by TbPLK contributes to the regulation of TbCentrin2 function and what protein phosphatase is responsible for TbCentrin2 dephosphorylation. KPP1 is potentially responsible for TbCentrin2 dephosphorylation (20), but this has not been experimentally verified. The previous work (22) and our current work suggest that regulation of centrin arm assembly in procyclic trypanosomes involves the phosphorylation of multiple centrin arm-localized proteins, such as TbCentrin2 and KIN-G, by TbPLK.

One of the intriguing questions is how TbPLK-phosphorylation of KIN-G negatively regulates the function of KIN-G. KIN-G is a microtubule plus end-directed motor protein, and its motor activity is required for cellular function (16), which suggests that KIN-G needs to travel along microtubules to execute its function. The best candidate microtubules that KIN-G may associate with are the specialized set of four microtubules (MtQ), which have their plus ends directed toward the distal tip of the cell in *T. brucei* (37, 38). Presumably, KIN-G may be first recruited to the centrin arm through binding to WDR2 (18) and then it associates with and travels along the MtQ to transport cargos in the centrin arm region to facilitate centrin arm assembly. In this regard, phosphorylated KIN-G is unable to bind to MtQ due to the loss of microtubule-binding activity (Figs. 2 and 3) and, hence, is unable to transport its cargos to their destinations. The lack of rescue of KIN-G RNAi by the expression of the phospho-mimic mutant KIN-G^{T301D} and the complete rescue of KIN-G RNAi by the expression of the phospho-deficient mutant KIN-G^{T301A} (Fig. 4) support this notion, and these findings further suggest that dephosphorylation of Thr301, but not phosphorylation of Thr301, is required for KIN-G function. The regulation of KIN-G function by TbPLK phosphorylation appears to be similar to the regulation of TbCentrin2 by TbPLK phosphorylation (22). The best candidate protein phosphatase for KIN-G dephosphorylation is the centrin arm-localized KPP1 (20), which also attenuates TbPLK kinase activity by dephosphorylating TbPLK at Thr125 (39).

We have provided evidence to demonstrate that phosphorylation of Thr301 in KIN-G disrupted its cellular function, causing defects in centrin arm assembly, FAZ elongation, flagellum positioning, cell division plane placement, cytokinesis, and Golgi biogenesis (Figs. 5-7), which mimics the defects caused by KIN-G RNAi (16). There is an intriguing question of why KIN-G appears to regulate so many cellular processes, while it only localizes to the centrin arm throughout the cell cycle (16). It should be noted that previous work showed that the deficiency in centrin arm integrity impairs FAZ elongation, flagellum positioning, cell division plane placement, cytokinesis, and Golgi biogenesis (11, 15, 16, 18, 19, 22). Since the proximal end of the FAZ is embedded within the hook complex between the centrin arm and the shank part of the hook complex (40) and assembly of the FAZ occurs from its proximal end (6, 7), the primary role of the centrin arm likely is to act as a hub to coordinate FAZ assembly. In this regard, all of the other defects described above, except Golgi biogenesis, are the secondary effects of the defective FAZ assembly. The impairment of Golgi biogenesis by the deficiency in centrin arm integrity led to the interpretation that centrin arm determines the site where Golgi is assembled (15), although the underlying mechanism has not been established. Presumably, there is a physical connection between the centrin arm and the Golgi apparatus, which may be mediated by the scaffold protein CAAP1, because CAAP1 resides in between the centrin arm and the Golgi apparatus and depletion of CAAP1

disconnects the two structures and disrupts Golgi biogenesis (16). All in all, it appears that deficiency in centrin arm integrity disrupts FAZ elongation and Golgi biogenesis, the former of which further causes flagellum mis-positioning, cell division plane mis-placement, and unequal cytokinesis. Therefore, the primary function of KIN-G is to regulate the formation of the centrin arm. Phosphorylation of Thr301 disrupts the microtubule-binding activity of KIN-G and, hence, the plus end-directed motility along the MtQ, suggesting that the regulation of centrin arm assembly by KIN-G requires its motor activity, in agreement with the results obtained with the expression of the motility-dead mutant KIN-G^{G266A} in KIN-G RNAi cells, which had almost identical phenotypes as the KIN-G^{T301D} complementation cells (16).

The defect in FAZ assembly due to defective centrin arm assembly, observed in KIN-G RNAi cells (16) and the KIN-G^{T301D} complementation cells (Fig. 7), is believed to be the cause of the mis-positioning of the newly synthesized flagellum and the mis-placement of the cell division plane. Previous work has demonstrated that positioning of the newly synthesized flagellum relies on the faithful duplication/segregation of its associated cytoskeletal structures, including the FAZ (14, 31). Elongation of the new FAZ appears to promote basal body migration (14), thereby facilitating flagellum segregation. The cell division plane in procyclic trypanosomes is placed along the longitudinal cell axis from the anterior tip of the NFD cell to the nascent posterior of the OFD cell (28), and its placement appears to depend on the length of the new flagellum (41) and the length of the new FAZ (14). However, the mis-placement of the cell division plane in CC2D RNAi cells containing a short-length new FAZ but a normal-length new flagellum (14) argues that it is the length of the new FAZ that determines the cell division plane. This notion is supported by the observed positive correlation between the length of the new FAZ and the length of the NFD cell in the control cells, CC2D RNAi cells (14), FAZ10 RNAi cells (42), KIN-G RNAi cells (16), and the KIN-G^{T301D} complementation cells (Fig. 6C). The mis-positioning of the new flagellum and the mis-placement of the cell division plane collectively contributed to the defects in cytokinesis and cell proliferation.

The complete rescue of KIN-G RNAi phenotypes by expression of the KIN-G^{T301A} mutant (Fig. 4) raised an interesting question about the role of TbPLK phosphorylation of KIN-G in trypanosome cells. TbPLK phosphorylates KIN-G throughout the entire protein, and Thr301 is one of the ten *in vitro* and *in vivo* phosphosites that was characterized in this work. Four other *in vitro* and *in vivo* phosphosites in the motor domain of KIN-G are located outside of the microtubule-binding motifs and the nucleotide-binding motifs (Fig. 1D); whether the phosphorylation/dephosphorylation of these sites may affect microtubule binding or nucleotide binding of KIN-G is unknown and remains to be explored. Five *in vitro* and *in vivo* phosphosites are located in the C-terminus of KIN-G, with three sites located in the three coiled-coil motifs and two sites located in the loop region between coiled-coil motifs #2 and #3 (Fig. 1D). The potential role of phosphorylation of these sites by TbPLK is also unknown and needs further exploration. However, because the C-terminal tail in kinesin proteins is known to bind cargo or cargo adaptor proteins (43), the phosphorylation of the five residues in the C-terminus of KIN-G may impact the binding of KIN-G to its cargo or cargo adaptor proteins. Future experiments will be

directed to exploring the potential biochemical and physiological roles of these phosphosites, which may uncover the other role(s) of TbPLK-mediated phosphorylation of KIN-G.

In summary, we have identified the orphan kinesin KIN-G as a substrate of TbPLK and demonstrated that phosphorylation of Thr301 by TbPLK disrupted KIN-G microtubule-binding activity. We further showed that expression of the phospho-mimic mutant KIN-G^{T301D} in trypanosome cells impaired the cellular function of KIN-G. Therefore, dephosphorylation of Thr301 in KIN-G is necessary for KIN-G to exert its function in regulating centrin arm assembly, thereby facilitating Golgi biogenesis and FAZ elongation, which further promotes flagellum positioning and cell division plane placement.

Materials and Methods

Trypanosome cell culture, RNAi, and complementation

The procyclic form of *T. brucei* strain Lister427 was cultured in the SDM-79 medium at 27°C. The KIN-G RNAi cell line, which was generated previously (16), was cultured in SDM-79 medium supplemented with 10% heat-inactivated fetal bovine serum (Sigma-Aldrich), 15 µg/ml G418, 50 µg/ml hygromycin, and 2.5 µg/ml phleomycin at 27°C. Cells were diluted with fresh medium whenever the cell density reached 5×10^{6}/ml. RNAi was induced with 1 µg/ml tetracycline, and cell growth was monitored daily with a hemacytometer.

The coding sequence of KIN-G was recoded to make it RNAi resistant, and the recoded KIN-G gene was cloned into pLew100-3HA-PAC vector. The pLew100-KIN-G-3HA-PAC plasmid was then used for site-directed mutagenesis to mutate the TbPLK-phosphorylated residues to aspartate or alanine, and then the resulting plasmids were used to transfect the KIN-G RNAi cell line. Transfectants were selected with 1 µg/ml puromycin in addition to 15 µg/ml G418, and 50 µg/ml hygromycin, and 2.5 µg/ml phleomycin, and then cloned by limiting dilution in a 96-well plate containing SDM-79 medium supplemented with appropriate antibiotics and 20% fetal bovine serum. Expression of recoded KIN-G and its phospho-mimic and phospho-deficient mutants, and knockdown of endogenous KIN-G were induced with 1 µg/ml tetracycline. Cell growth was monitored by daily counting of the cells with a hemacytometer.

In situ epitope tagging of proteins

Epitope tagging of KIN-G, KLIF, GB4, and Sec13 from their respective endogenous locus was carried out using the PCR-based method (44). KIN-G was tagged with a C-terminal triple HA epitope or PTP epitope, KLIF was tagged with a C-terminal triple HA epitope, GB4 was tagged with a C-terminal PTP epitope, and Sec13 was tagged with an N-terminal mCherry tag. Transfectants were selected with appropriate antibiotics, and clonal cell lines were obtained by limiting dilution in a 96-well plate as described above.

Immunofluorescence microscopy

To prepare intact trypanosome cells for immunofluorescence microscopy, cells were washed once with PBS, settled onto glass coverslips, fixed with methanol at -20°C for 30 min, and rehydrated with PBS at room

temperature. To prepare trypanosome cytoskeletons for immunofluorescence microscopy, cells were washed once with PBS, adhered onto glass coverslips, treated with 1% Nonidet-P40 in PEME buffer (100 mM PIPES, pH6.9, 2 mM EGTA, 1 mM MgSO4, and 0.1 mM EDTA) for 2 seconds at room temperature, and then fixed with cold methanol at -20°C for 30 min. Intact cells or cytoskeletons on the coverslips were incubated with the blocking buffer (3% BSA in PBS) at room temperature for 1 h, and then incubated with the primary antibody at room temperature for 1 h. The following primary antibodies were used: anti-HA monoclonal antibody (1:400 dilution, Sigma-Aldrich), anti-Protein A polyclonal antibody (1:400 dilution, Sigma-Aldrich), anti-CC2D polyclonal antibody (1:1,000 dilution) (14), 20H5 monoclonal antibody (1:400 dilution) (15), YL 1/2 monoclonal antibody (1: 1000 dilution) (25), anti-TbCentrin4/LdCentrin1 polyclonal antibody (1:1000 dilution) (45), anti-TbBILBO1 antibody (1: 400 dilution) (26), and anti-TbGRASP polyclonal antibody (1:400 dilution) (8). Cells or cytoskeletons on the glass coverslips were washed three times (5 min each) with PBS and incubated with secondary antibodies at room temperature for 1 h. The following secondary antibodies were used: FITC-conjugated anti-mouse IgG, FITC-conjugated anti-rabbit IgG, Cy3-conjugated anti-rabbit IgG, and Cy3-conjugated anti-rat IgG (all from MilliporeSigma). Cells or cytoskeletons were washed three times (5 min each) with PBS, mounted with DAPI-containing VectaShield mounting medium (Vector Labs), and imaged with the Olympus IX71 fluorescence microscope. Images were acquired and processed using the Slidebook 5 software.

Expression and purification of recombinant proteins

To express and purify recombinant proteins for *in vitro* microtubule-binding and gliding assays, KIN-G was cloned into the pET26 vector, and the resulting plasmid was used to generate the phospho-deficient and phospho-mimic mutants by site-directed mutagenesis. The full-length TbPLK was cloned into the pET41a vector, and the resulting plasmid was used to generate the kinase-dead mutant TbPLK^{K70R} by site-directed mutagenesis. These plasmids were each used to transform the *E. coli* BL21 strain. Expression of recombinant proteins was induced with 0.1 mM isopropyl β-d-thio-galactopyranoside at room temperature for KIN-G-6His and GST-TbPLK-6His and at 15°C overnight for GST-TbPLK^{K70R}-6His. Bacterial cells expressing KIN-G-6His and its mutants, GST-TbPLK-6His, and GST-TbPLK^{K70R}-6His were lysed by sonication in bacteria lysis buffer (50 mM NaH_2PO_4, 300 mM NaCl, 10 mM imidazole, pH 8.0), and cell lysate was cleared by centrifugation at 20,000 ×*g* for 10 min at 4°C. Cleared cell lysate was incubated with the Chelating Sepharose Fast Flow (GE Healthcare) beads charged with nickel ion at 4°C for 30 min. Beads were washed five times with 1 ml wash buffer (50 mM NaH_2PO_4, 1 M NaCl, 120 mM imidazole, pH 8.0) for each wash. Recombinant proteins were eluted with elution buffer (50 mM NaH_2PO_4, 300 mM NaCl, 250 mM imidazole, pH 8.0), and eluted proteins were concentrated and buffer-exchanged to the kinase assay buffer (10 mM HEPES, pH 7.5, 10 mM MgCl2, 50 mM NaCl, 1 mM EGTA, 1 mM DTT) with Amicon Ultra Centrifugal Filters 10K (MilliporeSigma).

***In vitro* kinase assay using the thiophosphorylation method**

In vitro kinase assay was performed by using a semisynthetic epitope to detect thiophosphorylated kinase substrates (24). Purified recombinant proteins were incubated in the kinase assay buffer (10 mM HEPES pH7.5, 10 mM $MgCl_2$, 50 mM NaCl, and 0.4 mM DTT) supplemented with 1 mM ATP-γ-S at room temperature for 30 min. 50 mM p-nitrobenzyl mesylate (PNBM), which alkylates thiophosphates to form thiophosphate ester epitopes that can be recognized by the anti-thiophosphate ester antibody, was added to the kinase reaction and was incubated at room temperature for 60 min. Thiophosphorylated proteins were separated by SDS-PAGE, transferred onto a PVDF membrane, and then immunoblotted with the anti-thiophosphate ester (anti-ThioP) monoclonal antibody (1:5,000 dilution, ThermoFisher).

Identification of TbPLK-phosphosites in KIN-G by mass spectrometry

Purified recombinant KIN-G-6His was mixed with purified recombinant GST-TbPLK-6His in the kinase assay buffer (see above) containing 0.2 mM ATP at room temperature for 30 min. Thiophosphorylated proteins were separated by SDS-PAGE and stained with coomassie blue dye. The gel slice containing the phosphorylated KIN-G-6His band was excised, and incubated with 160 ng trypsin at 37°C for 4 h, according to published procedures (46). Peptides were extracted with 50 ml of 50% acetonitrile and 5% formic acid, dried using SpeedVac, resuspended in 2% acetonitrile and 0.1% formic acid, and injected onto Thermo LTQ Orbitrap XL (ThermoFisher Scientific), according to published procedures (47). Peptide samples were analyzed on an LTQ Orbitrap XL interfaced with an Eksigent nano-LC 2D plus ChipLC system (Eksigent Technologies). Samples were loaded onto a ChromXP C18-CL trap column (200 mm i.d. x 0.5 mm length) at a flow rate of 3 nL/min. Reverse-phase C18 chromatographic separation of peptides was carried on a ChromXP C18-CL column (75 mm i.d x 10 cm length) at 300 nL/min. The LTQ Orbitrap was operated in a data-dependent mode to simultaneously measure full-scan MS spectra in the Orbitrap and the five most intense ions in the LTQ by CID, respectively. In each cycle, MS1 was acquired at a target value of 1E6 with a resolution of 100,000 (m/z 400) followed by top five MS2 scan at a target value of 3E4. The mass spectrometric setting was: spray voltage at 1.6 KV, and charge state screening and rejection of singly charged ion enabled. Ion selection thresholds were set at 8,000 for MS2, 35% normalized collision energy, activation Q was set at 0.25, and dynamic exclusion was employed for 30 sec. Raw data files were processed and searched against the *T. brucei* proteome database using the Mascot and Sequest HT (version 13) search engines. The search conditions were set as follows: peptide tolerance of 10 p.p.m. and MS/MS tolerance of 0.8 Da, with two missed cleavages permitted and the enzyme set as trypsin.

Tubulin polymerization and microtubule binding and gliding assay

In vitro tubulin polymerization was performed according to our published procedure (48). Non-labeled porcine brain tubulin (Cytoskeleton, Inc., Cat#: T240-A80, 80 μg) was mixed with rhodamine-labeled porcine brain tubulin (Cytoskeleton, Inc., Cat#: TL590M, 20 μg) in BRB80-DTT buffer (80 mM Potassium-PIPES, pH 6.8, 1 mM $MgCl_2$, 1 mM EGTA, 1 mM DTT) supplemented with 1 mM Guanylyl-(α,β)-methylene-

diphosphonate (GMP-CPP). The mixture was incubated at 4°C for 5 min and then clarified by centrifugation at 353,000 ×*g* at 4°C for 5 min in a TLA120.1 rotor in an ultracentrifuge (Beckman Coulter TL-100) to remove aggregates. The supernatant was snap-frozen in liquid nitrogen, aliquoted, and stored at -80°C. To generate microtubule seeds, an aliquot of the supernatant was diluted (1:4 v/v) with the BRB80-DTT buffer to a final concentration of 0.5 mg/ml, and incubated at 37°C for 30 min. Microtubule seeds were centrifugated at 353,000 ×*g* at 27°C for 5 min, and the pellet was resuspended in the BRB80-DTT buffer.

To polymerize microtubules from the microtubule seeds, 20 μg of rhodamine-labeled tubulin was mixed with the microtubule seeds in the presence of 1 mM GTP. Microtubules were then successively assembled by incubating at 37°C in the BRB80-DTT-GTP buffer (BRB80-DTT buffer, 1.0 mM GTP) with 0.1 μM Taxol for 20 min, 1 μM Taxol for 10 min, and 10 μM Taxol for 20 min. Assembled microtubules were diluted with 10 μM Taxol in the BRB80-DTT-GTP buffer.

Microtubule-binding and -gliding assay was conducted in a chamber assembled on a glass slide with two double-sided tapes, which were spaced 8 mm apart, and covered with a 22 mm × 30 mm cover glass. Twenty microliters of 3 μM recombinant KIN-G-6His or its mutants, which were suspended in the BRB80-DTT-ATP-Taxol buffer containing 800 ng/ml BSA, was loaded into the chamber and incubated for 3 min to allow the attachment of KIN-G-6His to the cover glass. The chamber was washed twice with 20 μl of the BRB80-DTT-ATP-Taxol buffer, and 20 μl of 120 nM rhodamine-labeled microtubules in the BRB80-DTT-ATP-Taxol buffer containing 2.25 mg/ml BSA was then loaded into the chamber. After incubation for 2 min, the chamber was observed for microtubule binding and gliding under the Nikon A1 confocal microscope, and images were captured every 5 seconds. Movie files of the AVI format were generated by NIS Elements (Nikon).

To test the effect of TbPLK phosphorylation on KIN-G microtubule binding and gliding, two experiments were performed. In experiment #1, 4 μM recombinant KIN-G-6His was pre-incubated with 2 μM GST-TbPLK-6His or GST-TbPLK^{K70R}-6His in the presence of 1 mM ATP at 37°C for 7 min, and the protein mixture was clarified by centrifugation at 21,000 ×*g* for 30 sec. The supernatant was used for microtubule-binding and -gliding assay as described above. In experiment #2, 4 μM recombinant KIN-G-6His was settled onto glass coverslip in the chamber. Microtubules were then added into the chamber, and incubated for 5 min. Subsequently, 0.2 μM GST-TbPLK-6xHis or the BRB80-DTT-ATP-Taxol buffer was added into the chamber, and image acquisition was started after 2 min of incubation in the Nikon A1 confocal microscope.

Microtubules bound to KIN-G or its mutants were quantified in the last image of the time-lapse imaging process or at the indicated time point of the time-lapse imaging process. Nonspecifically coverslip-attached microtubules, which showed no gliding during the time-lapse imaging process, were not counted as KIN-G-bound microtubules and, thus, were excluded. Microtubule-gliding speed was calculated using the microtubules that exhibited continuous movement for at least 100 sec (20 frames) in time-lapse imaging.

Acknowledgements: We are grateful to Dr. Cynthia Y. He of National University of Singapore for providing anti-CC2D antibody and anti-TbGRASP antibody, Dr. Derrick Robinson of University of Bordeaux for

providing anti-TbBILBO1 antibody, and Dr. Hira Nakhasi of the FDA for providing anti-TbCentrin4/LdCen1 antibody. This work was supported by the NIH R01 grants AI118736 and AI101437 to Z. L. The funders do not play any role in the study design, data collection and analysis, decision to publish, or preparation of the manuscript.

Competing interests: The authors declare that they have no conflicts of interest with the contents of this article.

Author contributions: Yasuhiro Kurasawa: Conceptualization, Methodology, Visualization, Investigation, Formal analysis, Writing – Reviewing and Editing. **Qing Zhou:** Methodology, Visualization, Investigation, Formal analysis, Writing – Reviewing and Editing. **Kyu Joon Lee**: Methodology, Visualization, Investigation, Writing – Reviewing and Editing. **Huiqing Hu**: Methodology, Visualization, Investigation, Writing – Reviewing and Editing. **Ziyin Li***:* Conceptualization, Supervision, Project administration, Funding acquisition, Writing – Original Draft; Writing – Reviewing and Editing.

References:

1. Sunter JD, Gull K. 2016. The Flagellum Attachment Zone: 'The Cellular Ruler' of Trypanosome Morphology. Trends Parasitol 32:309-24.
2. Lacomble S, Vaughan S, Gadelha C, Morphew MK, Shaw MK, McIntosh JR, Gull K. 2009. Three-dimensional cellular architecture of the flagellar pocket and associated cytoskeleton in trypanosomes revealed by electron microscope tomography. J Cell Sci 122:1081-90.
3. Esson HJ, Morriswood B, Yavuz S, Vidilaseris K, Dong G, Warren G. 2012. Morphology of the trypanosome bilobe, a novel cytoskeletal structure. Eukaryot Cell 11:761-72.
4. Morriswood B. 2015. Form, Fabric, and Function of a Flagellum-Associated Cytoskeletal Structure. Cells 4:726-47.
5. Vaughan S, Gull K. 2016. Basal body structure and cell cycle-dependent biogenesis in *Trypanosoma brucei*. Cilia 5:5.
6. Sunter JD, Varga V, Dean S, Gull K. 2015. A dynamic coordination of flagellum and cytoplasmic cytoskeleton assembly specifies cell morphogenesis in trypanosomes. J Cell Sci 128:1580-94.
7. Zhou Q, Hu H, He CY, Li Z. 2015. Assembly and maintenance of the flagellum attachment zone filament in *Trypanosoma brucei*. J Cell Sci 128:2361-72.
8. He CY, Ho HH, Malsam J, Chalouni C, West CM, Ullu E, Toomre D, Warren G. 2004. Golgi duplication in *Trypanosoma brucei*. J Cell Biol 165:313-21.
9. Bangs JD. 2011. Replication of the ERES:Golgi junction in bloodstream-form African trypanosomes. Mol Microbiol 82:1433-43.
10. Abeywickrema M, Vachova H, Farr H, Mohr T, Wheeler RJ, Lai DH, Vaughan S, Gull K, Sunter JD, Varga V. 2019. Non-equivalence in old- and new-flagellum daughter cells of a proliferative division in Trypanosoma brucei. Mol Microbiol 112:1024-1040.
11. Zhou Q, Gheiratmand L, Chen Y, Lim TK, Zhang J, Li S, Xia N, Liu B, Lin Q, He CY. 2010. A comparative proteomic analysis reveals a new bi-lobe protein required for bi-lobe duplication and cell division in *Trypanosoma brucei*. PLoS ONE 5:e9660.
12. Pham KTM, Hu H, Li Z. 2020. Maintenance of hook complex integrity and centrin arm assembly facilitates flagellum inheritance in Trypanosoma brucei. J Biol Chem 295:12962-12974.
13. Hu H, Zhou Q, Li Z. 2015. A Novel Basal Body Protein That Is a Polo-like Kinase Substrate Is Required for Basal Body Segregation and Flagellum Adhesion in *Trypanosoma brucei*. J Biol Chem 290:25012-22.

14. Zhou Q, Liu B, Sun Y, He CY. 2011. A coiled-coil- and C2-domain-containing protein is required for FAZ assembly and cell morphology in *Trypanosoma brucei*. J Cell Sci 124:3848-58.
15. He CY, Pypaert M, Warren G. 2005. Golgi duplication in *Trypanosoma brucei* requires Centrin2. Science 310:1196-8.
16. Zhou Q, Kurasawa Y, Hu H, Souza Onofre T, Li Z. 2024. An orphan kinesin in Trypanosoma brucei regulates hook complex assembly and Golgi biogenesis. mBio doi:10.1128/mbio.02634-24:e0263424.
17. Pham KTM, Zhou Q, Kurasawa Y, Li Z. 2019. BOH1 cooperates with Polo-like kinase to regulate flagellum inheritance and cytokinesis initiation in *Trypanosoma brucei*. J Cell Sci 132:jcs230581.
18. Zhou Q, Hu H, Li Z. 2025. WDR2 regulates the orphan kinesin KIN-G to promote hook complex and Golgi biogenesis in Trypanosoma brucei. mBio 16:e0037125.
19. de Graffenried CL, Ho HH, Warren G. 2008. Polo-like kinase is required for Golgi and bilobe biogenesis in *Trypanosoma brucei*. J Cell Biol 181:431-8.
20. Zhou Q, Dong G, Li Z. 2018. Flagellum inheritance in *Trypanosoma brucei* requires a kinetoplastid-specific protein phosphatase. J Biol Chem 293:8508-8520.
21. Hu H, Zhou Q, Han X, Li Z. 2017. $CRL4^{WDR1}$ Controls Polo-like Kinase Protein Abundance to Promote Bilobe Duplication, Basal Body Segregation and Flagellum Attachment in *Trypanosoma brucei*. PLoS Pathog 13:e1006146.
22. de Graffenried CL, Anrather D, Von Raussendorf F, Warren G. 2013. Polo-like kinase phosphorylation of bilobe-resident TbCentrin2 facilitates flagellar inheritance in *Trypanosoma brucei*. Mol Biol Cell 24:1947-63.
23. Nett IR, Martin DM, Miranda-Saavedra D, Lamont D, Barber JD, Mehlert A, Ferguson MA. 2009. The phosphoproteome of bloodstream form *Trypanosoma brucei*, causative agent of African sleeping sickness. Mol Cell Proteomics 8:1527-38.
24. Allen JJ, Li M, Brinkworth CS, Paulson JL, Wang D, Hubner A, Chou WH, Davis RJ, Burlingame AL, Messing RO, Katayama CD, Hedrick SM, Shokat KM. 2007. A semisynthetic epitope for kinase substrates. Nat Methods 4:511-6.
25. Woods A, Sherwin T, Sasse R, MacRae TH, Baines AJ, Gull K. 1989. Definition of individual components within the cytoskeleton of *Trypanosoma brucei* by a library of monoclonal antibodies. J Cell Sci 93 (Pt 3):491-500.
26. Bonhivers M, Nowacki S, Landrein N, Robinson DR. 2008. Biogenesis of the trypanosome endo-exocytotic organelle is cytoskeleton mediated. PLoS Biol 6:e105.
27. Zhou Q, An T, Pham KTM, Hu H, Li Z. 2018. The CIF1 protein is a master orchestrator of trypanosome cytokinesis that recruits several cytokinesis regulators to the cytokinesis initiation site. J Biol Chem 293:16177-16192.
28. Wheeler RJ, Scheumann N, Wickstead B, Gull K, Vaughan S. 2013. Cytokinesis in *Trypanosoma brucei* differs between bloodstream and tsetse trypomastigote forms: implications for microtubule-based morphogenesis and mutant analysis. Mol Microbiol 90:1339-55.
29. Rindisbacher L, Hemphill A, Seebeck T. 1993. A repetitive protein from Trypanosoma brucei which caps the microtubules at the posterior end of the cytoskeleton. Mol Biochem Parasitol 58:83-96.
30. Kurasawa Y, An T, Li Z. 2020. Polo-like kinase in trypanosomes: an odd member out of the Polo family. Open Biol 10:200189.
31. Ikeda KN, de Graffenried CL. 2012. Polo-like kinase is necessary for flagellum inheritance in *Trypanosoma brucei*. J Cell Sci 125:3173-84.
32. Lozano-Nunez A, Ikeda KN, Sauer T, de Graffenried CL. 2013. An analogue-sensitive approach identifies basal body rotation and flagellum attachment zone elongation as key functions of PLK in *Trypanosoma brucei*. Mol Biol Cell 24:1321-33.
33. Li Z, Umeyama T, Li Z, Wang CC. 2010. Polo-like kinase guides cytokinesis in *Trypanosoma brucei* through an indirect means. Eukaryot Cell 9:705-16.
34. Kumar P, Wang CC. 2006. Dissociation of cytokinesis initiation from mitotic control in a eukaryote. Eukaryot Cell 5:92-102.
35. Hammarton TC, Kramer S, Tetley L, Boshart M, Mottram JC. 2007. *Trypanosoma brucei* Polo-like kinase is essential for basal body duplication, kDNA segregation and cytokinesis. Mol Microbiol 65:1229-48.

36. Kurasawa Y, Lee KJ, Hu H, Pham KTM, Li Z. 2022. Polo-like kinase and Aurora B kinase phosphorylate and cooperate with the CIF1-CIF2 complex to promote cytokinesis initiation in Trypanosoma brucei. Open Biol 12:220197.
37. Robinson DR, Sherwin T, Ploubidou A, Byard EH, Gull K. 1995. Microtubule polarity and dynamics in the control of organelle positioning, segregation, and cytokinesis in the trypanosome cell cycle. J Cell Biol 128:1163-72.
38. Gull K. 1999. The cytoskeleton of trypanosomatid parasites. Annu Rev Microbiol 53:629-55.
39. An T, Hu H, Li Z. 2021. The kinetoplastid-specific phosphatase KPP1 attenuates PLK activity to facilitate flagellum inheritance in Trypanosoma brucei. Sci Signal 14:eabc6435.
40. Morriswood B, Havlicek K, Demmel L, Yavuz S, Sealey-Cardona M, Vidilaseris K, Anrather D, Kostan J, Djinovic-Carugo K, Roux KJ, Warren G. 2013. Novel bilobe components in *Trypanosoma brucei* identified using proximity-dependent biotinylation. Eukaryot Cell 12:356-67.
41. Kohl L, Robinson D, Bastin P. 2003. Novel roles for the flagellum in cell morphogenesis and cytokinesis of trypanosomes. Embo J 22:5336-46.
42. Moreira BP, Fonseca CK, Hammarton TC, Baqui MM. 2017. Giant FAZ10 is required for flagellum attachment zone stabilization and furrow positioning in *Trypanosoma brucei*. J Cell Sci 130:1179-1193.
43. Hirokawa N, Noda Y, Okada Y. 1998. Kinesin and dynein superfamily proteins in organelle transport and cell division. Curr Opin Cell Biol 10:60-73.
44. Shen S, Arhin GK, Ullu E, Tschudi C. 2001. *In vivo* epitope tagging of *Trypanosoma brucei* genes using a one step PCR-based strategy. Mol Biochem Parasitol 113:171-3.
45. Selvapandiyan A, Kumar P, Morris JC, Salisbury JL, Wang CC, Nakhasi HL. 2007. Centrin1 is required for organelle segregation and cytokinesis in *Trypanosoma brucei*. Mol Biol Cell 18:3290-301.
46. Rosenfeld J, Capdevielle J, Guillemot JC, Ferrara P. 1992. In-gel digestion of proteins for internal sequence analysis after one- or two-dimensional gel electrophoresis. Anal Biochem 203:173-9.
47. Lee KJ, Li Z. 2021. The CRK2-CYC13 complex functions as an S-phase cyclin-dependent kinase to promote DNA replication in Trypanosoma brucei. BMC Biol 19:29.
48. Hu H, Kurasawa Y, Zhou Q, Li Z. 2024. A kinesin-13 family kinesin in Trypanosoma brucei regulates cytokinesis and cytoskeleton morphogenesis by promoting microtubule bundling. PLoS Pathog 20:e1012000.

Figure Legends:

Figure 1. KIN-G is a substrate of TbPLK in *T. brucei*. (**A**). Co-immunostaining of KIN-G-3HA and TbPLK during the cell cycle in the procyclic form. Open arrowheads indicate KIN-G signal at the centrin arm. TbPLK signal at different structures are indicated. BB: basal body; CA: centrin arm; FC: flagella connector; FAZt: FAZ tip. Scale bars: 5 μm. (**B**). TbPLK phosphorylates KIN-G *in vitro*. The asterisk indicates a non-specific band. (**C**). *In vitro* phosphorylated KIN-G migrates slower than non-phosphorylated KIN-G on SDS-PAGE. (**D**). *In vitro* TbPLK phosphosites on KIN-G protein identified by mass spectrometry. Phosphosites highlighted in red indicate the *in vitro* and *in vivo* phosphosites. MD: motor domain; CC: coiled coil; MB: microtubule-binding motif; NB: nucleotide-binding motif. (**E**). Phosphosites within the KIN-G protein sequence spanning MB1 to MB3. Sequences highlighted in blue indicate the microtubule-binding motifs (MB1, MB2 and MB3), and sequences highlighted in green indicate the nucleotide-binding motifs (NB2 and NB3). Phosphosites highlighted in red in the yellow box indicate the *in vitro* and *in vivo* phosphosites.

Figure 2. Phosphorylation of KIN-G by TbPLK disrupts the microtubule-binding activity of KIN-G. (**A**). Pre-incubation of KIN-G with TbPLK, but not TbPLK^{K70R}, disrupted KIN-G microtubule-binding activity. KIN-

G, KIN-G and TbPLK mixture, and KIN-G and TbPLK^{K70R} mixture were first attached to coverslips and then microtubules (MTs) were added into the chamber. (**B**). Quantitation of KIN-G-bound microtubules in the presence or absence of TbPLK or in the presence of TbPLK^{K70R}. Error bars indicate S.D. from three independent experiments. ****: $p<0.0001$; ns: no significance (one-way ANOVA). (**C**). Measurement of the microtubule-gliding speed of KIN-G in the presence or absence of TbPLK or in the presence of TbPLK^{K70R}. Error bars indicate S.D. from three independent experiments. ND: not done. ns: no significance (one-way ANOVA). (**D**). TbPLK disrupted KIN-G microtubule-binding activity. KIN-G was first attached to coverslips, MTs were added into the chamber, and finally TbPLK was added into the chamber. (**E**). Quantitation of KIN-G-bound microtubules following the incubation with or without TbPLK. Error bars indicate S.D. from three independent experiments. **: $p<0.01$; ***: $p<0.001$ (Student's *t*-test).

Figure 3. Phosphorylation of Thr301 on KIN-G by TbPLK disrupts the microtubule-binding activity of KIN-G. (**A**). Microtubule-binding activity of KIN-G and its Thr284 and Thr301 mutants. (**B**). Quantitation of the bound microtubules of KIN-G and its mutants. Error bars indicate S.D. from three independent experiments. **: $p<0.01$; ns: no significance (one-way ANOVA). (**C**). Measurement of the microtubule-gliding speed of KIN-G and its mutants. Error bars indicate S.D. from three independent experiments. ND: not done. ns: no significance (one-way ANOVA).

Figure 4. Expression of Thr301 phospho-mimic mutant of KIN-G disrupts cell proliferation. (A). Subcellular localization of ectopically expressed KIN-G, KIN-G^{T301A}, KIN-G^{T301D}, co-stained with TbCentrin4. BB: basal body; CA: centrin arm. Scale bar: 5 μm. (**B**). Western blotting to detect the levels of ectopically 3HA-tagged KIN-G and its mutants and the endogenously PTP-tagged KIN-G before and after tetracycline induction for 48 hours. TbPSA6 serves as a loading control. (**C**). Growth curves of KIN-G RNAi cell line and its complementation cell lines expressing KIN-G, KIN-G^{T301A}, or KIN-G^{T301D}. OE: overexpression. Error bars indicate S.D. from three independent experiments. (**D**). Quantitation of the numbers of nuclei (N) and kinetoplasts (K) of KIN-G RNAi cell line and its complementation cell lines. Error bars indicated S.D. from three independent experiments.

Figure 5. TbPLK phosphorylation of Thr301 on KIN-G disrupts centrin arm and Golgi biogenesis. (**A**). Effect of the expression of KIN-G^{T301D} on centrin arm formation. Cells were co-immunostained with the pan-centrin antibody 20H5 and the anti-TbCentrin4 antibody. Scale bar: 5 μm. (**B**). Measurement of centrin arm length in KIN-G RNAi cells expressing Thr301 phospho-mimic of KIN-G before and after tetracycline induction. Error bars indicate S.D. ns: no significance; ****: $p<0.0001$ (Student's *t*-test). (**C**). Effect of the expression of KIN-G^{T301D} on the biogenesis of Golgi and ER exit site (ERES). Cells were co-immunostained with the anti-TbGRASP antibody to detect TbGRASP. ERES was labeled by mCherry-tagged Sec13. Scale bar:

5 μm. (**D**). Quantitation of cells with different numbers of Golgi/ERES in control and KIN-G RNAi cells. Error bars indicate S.D. from three independent experiments. ***: $p<0.001$; ****: $p<0.0001$ (one-way ANOVA).

Figure 6. TbPLK phosphorylation of Thr301 on KIN-G impairs flagellar inheritance. (**A**). Effect of the expression of KIN-G^{T301D} on the elongation of the flagellum attachment zone (FAZ) filament. Cells were immunostained with the anti-CC2D antibody. Scale bar: 5 μm. (**B**). Measurement of the length of the new and the old FAZ filaments in control and KIN-G RNAi cells expressing KIN-G^{T301D}. Error bars indicate S.D. **: $p<0.01$; ****: $p<0.0001$ (one-way ANAVA). (**C**). Measurement of the cell body length of the new-flagellum daughter (NFD) cell and its correlation with the length of the new FAZ for control cells and KIN-G RNAi cells expressing KIN-G^{T301D}. (**D**). Effect of the expression of KIN-G^{T301D} on the segregation of flagellar pocket collar (FPC) and basal body (BB). Cells were co-immunostained with anti-TbBILBO1 antibody and YL1/2 antibody. Scale bar: 5 μm. (**E, F**). Measurement of the inter-FPC distance (**E**) and inter-BB distance (**F**) in control cells and KIN-G RNAi cells expressing Thr301 phospho-mimic mutant of KIN-G. Error bars indicate S.D. ****: $p<0.0001$ (one-way ANOVA).

Figure 7. Phosphorylation of KIN-G at Thr301 by TbPLK disrupts cell division plane placement. (**A**). Immunofluorescence microscopy to detect the cell division plane with endogenous triple HA-tagged KLIF in dividing cells from non-induced control and KIN-G RNAi cells. Yellow arrows indicate the KLIF-marked cell division plane. NFD: new-flagellum daughter; OFD: old-flagellum daughter. Scale bar: 5 μm. (**B**). Immunofluorescence microscopy to detect the NFD posterior and the OFD nascent posterior with PTP-tagged GB4 protein. Scale bar: 5 μm. (**C**). Measurement of the inter-posterior distance of bi-nucleated cells from non-induced control and KIN-G RNAi cells. Error bars indicate S.D. ***, $p<0.001$ (Student's *t*-test). (**D**). Non-induced and tetracycline-induced KIN-G RNAi cells expressing KIN-G^{T301D}. Shown are a non-dividing cell without a visible cleavage furrow and three dividing cells with a visible cleavage furrow. Yellow arrows indicate the cell division plane. Scale bar: 5 μm. (**E**). Quantitation of bi-nucleated cells with or without a visible cleavage furrow from non-induced and tetracycline-induced KIN-G RNAi cells expressing KIN-G^{T301D}. Error bars indicate S.D. from three independent experiments. . ****, $p<0.0001$ (one-way ANOVA). (**F**). Percentage of dividing bi-nucleated cells with a normally placed cell division plane or an abnormally placed cell division plane from non-induced and tetracycline-induced KIN-G RNAi cells expressing KIN-G^{T301D}.

Figure 1

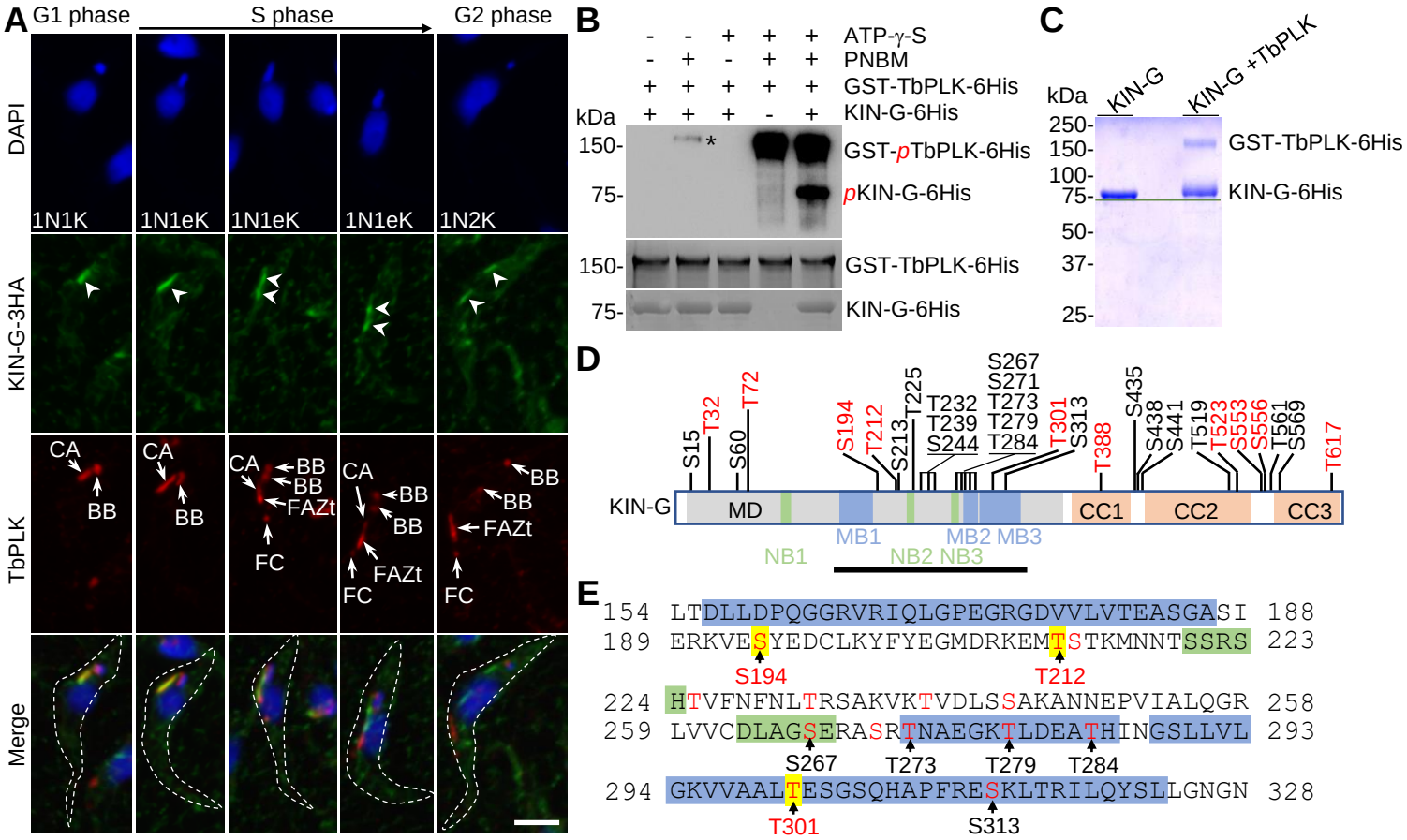
A
G1 phase
S phase
G2 phase
DAPI
KIN-G-3HA
TbPLK
Merge
1N1K
1N1eK
1N1eK
1N1eK
1N2K
CA
BB
FAZt
FC
B
ATP-γ-S
PNBM
GST-TbPLK-6His
KIN-G-6His
kDa
150-
75-
GST-pTbPLK-6His
pKIN-G-6His
GST-TbPLK-6His
KIN-G-6His
C
KIN-G
KIN-G +TbPLK
kDa
250-
150-
100-
75-
50-
37-
25-
GST-TbPLK-6His
KIN-G-6His
D
S15
T32
T72
S60
S194
T212
S213
T225
T232
T239
S244
S267
S271
T273
T279
T284
T301
S313
T388
S435
S438
S441
T519
T523
S553
S556
T561
S569
T617
KIN-G
MD
CC1
CC2
CC3
NB1
MB1
NB2
MB2
NB3
MB3
E
154 LTDLLDPQGGRVRIQLGPEGRGDVVLVTEASGASI 188
189 ERKVESYEDCLKYFYEGMDRKEMTSTKMNNTSSRS 223
S194
T212
224 HTVFNFNLTRSAKVKTVDLSSAKANNEPVIALQGR 258
259 LVVCDLAGSERASRTNAEGKTLDEATHINGSLLVL 293
S267
T273
T279
T284
294 GKVVAALTESGSQHAPFRESKLTRILQYSLLGNGN 328
T301
S313

Figure 2

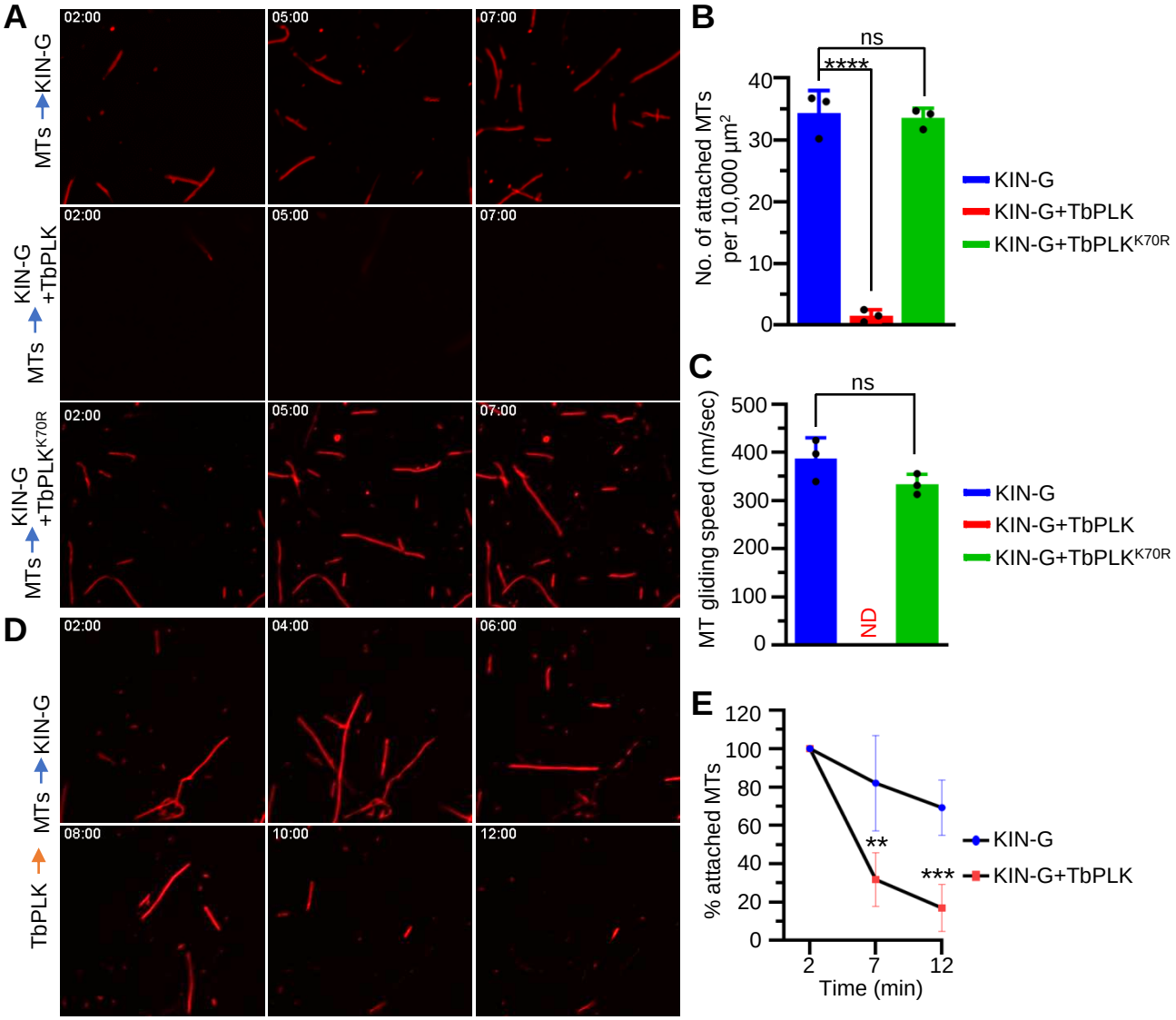
A
MTs
KIN-G
KIN-G +TbPLK
KIN-G +TbPLK^{K70R}
02:00
05:00
07:00
B
ns
****
No. of attached MTs per 10,000 µm^2
0
10
20
30
40
KIN-G
KIN-G+TbPLK
KIN-G+TbPLK^{K70R}
C
ns
MT gliding speed (nm/sec)
0
100
200
300
400
500
ND
KIN-G
KIN-G+TbPLK
KIN-G+TbPLK^{K70R}
D
TbPLK
02:00
04:00
06:00
08:00
10:00
12:00
E
% attached MTs
0
20
40
60
80
100
120
**
***
2
7
12
Time (min)
KIN-G
KIN-G+TbPLK

Figure 3

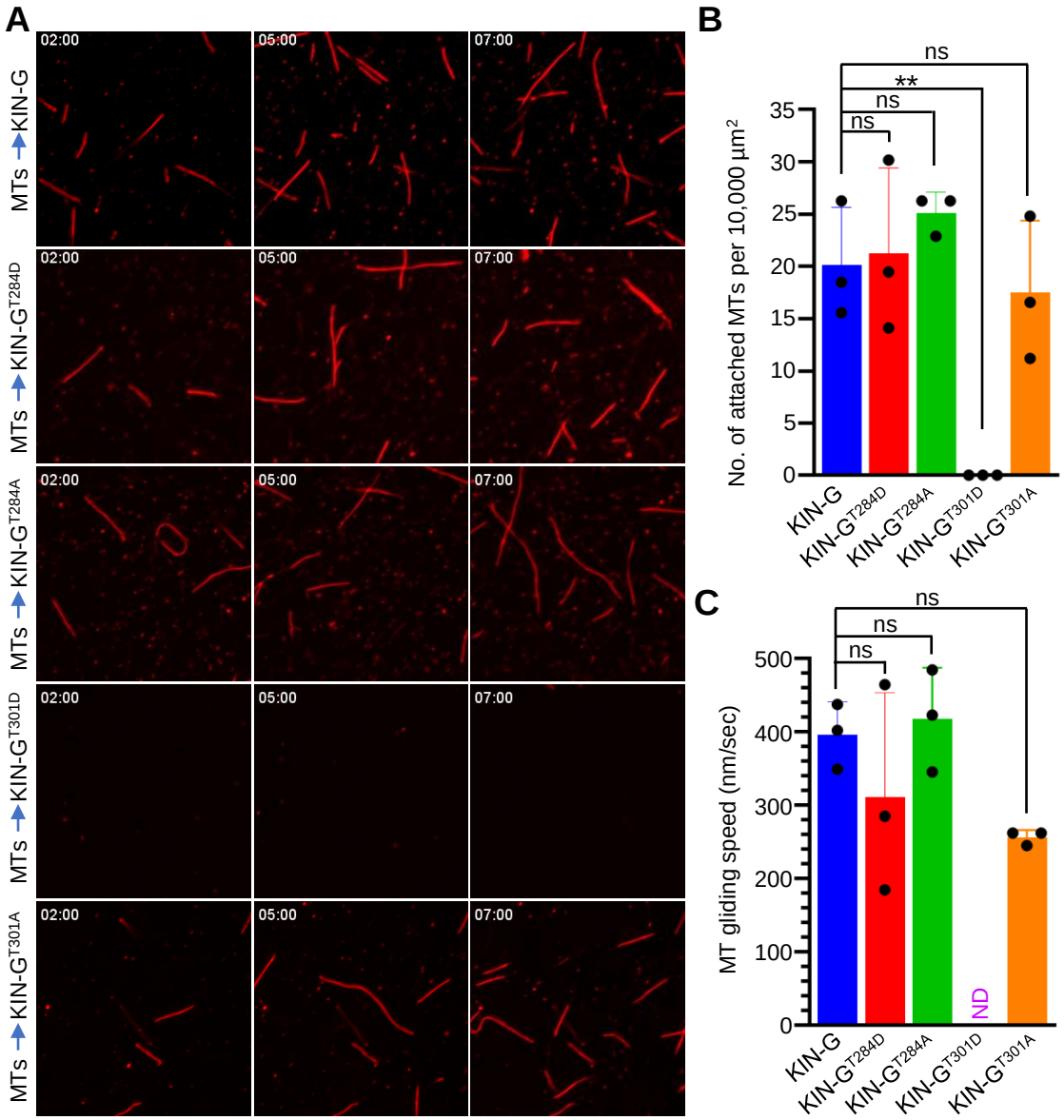
A
MTs → KIN-G
MTs → KIN-G^{T284D}
MTs → KIN-G^{T284A}
MTs → KIN-G^{T301D}
MTs → KIN-G^{T301A}
02:00
05:00
07:00
B
No. of attached MTs per 10,000 µm^2
0
5
10
15
20
25
30
35
ns
ns
ns
**
KIN-G
KIN-G^{T284D}
KIN-G^{T284A}
KIN-G^{T301D}
KIN-G^{T301A}
C
MT gliding speed (nm/sec)
0
100
200
300
400
500
ns
ns
ns
ND
KIN-G
KIN-G^{T284D}
KIN-G^{T284A}
KIN-G^{T301D}
KIN-G^{T301A}

Figure 4

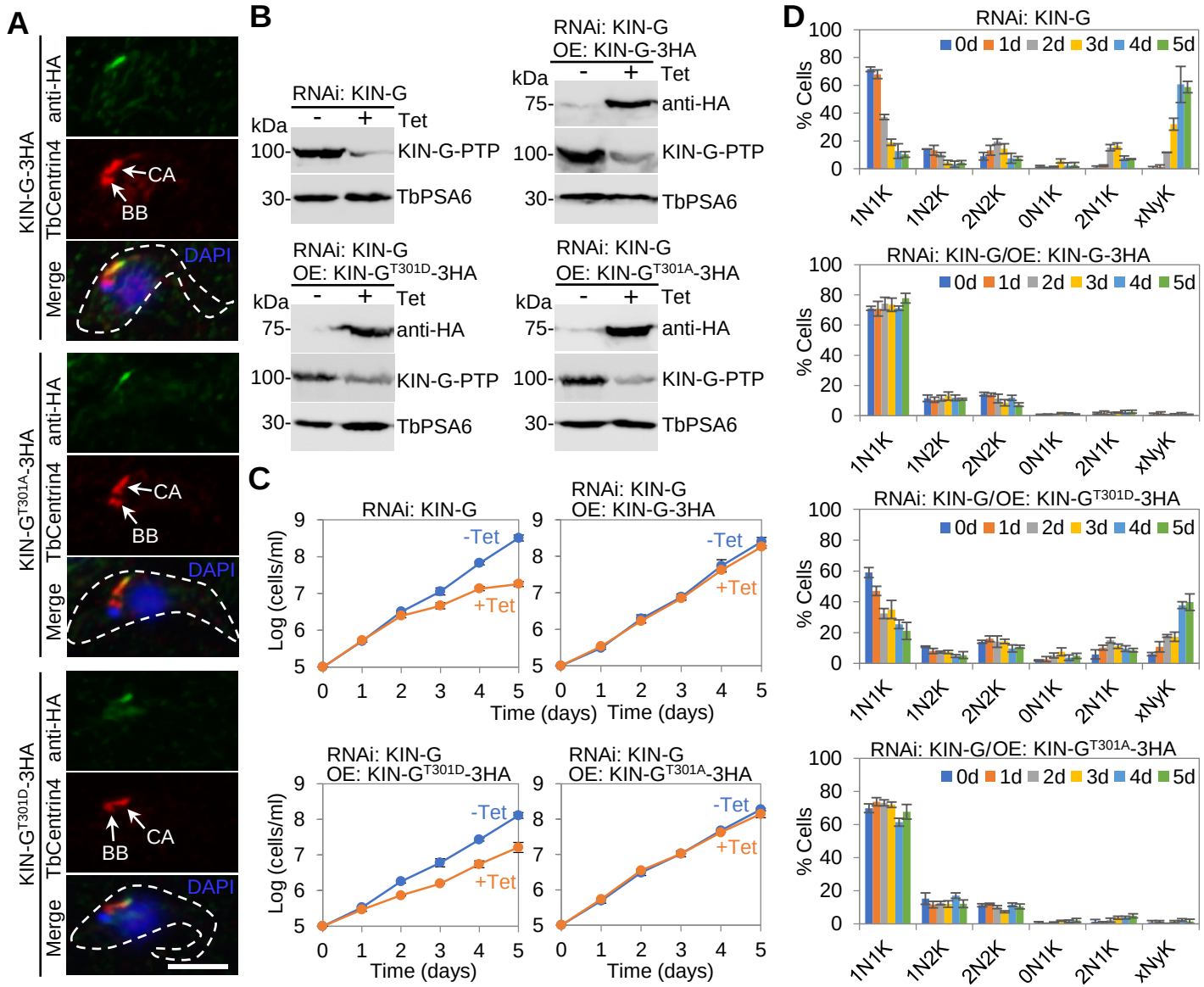
A
KIN-G-3HA
KIN-G^{T301A}-3HA
KIN-G^{T301D}-3HA
anti-HA
TbCentrin4
Merge
CA
BB
DAPI
B
RNAi: KIN-G
RNAi: KIN-G OE: KIN-G-3HA
RNAi: KIN-G OE: KIN-G^{T301D}-3HA
RNAi: KIN-G OE: KIN-G^{T301A}-3HA
kDa
Tet
KIN-G-PTP
TbPSA6
anti-HA
C
Log (cells/ml)
Time (days)
-Tet
+Tet
D
% Cells
0d 1d 2d 3d 4d 5d
1N1K
1N2K
2N2K
0N1K
2N1K
xNyK
RNAi: KIN-G
RNAi: KIN-G/OE: KIN-G-3HA
RNAi: KIN-G/OE: KIN-G^{T301D}-3HA
RNAi: KIN-G/OE: KIN-G^{T301A}-3HA

Figure 5

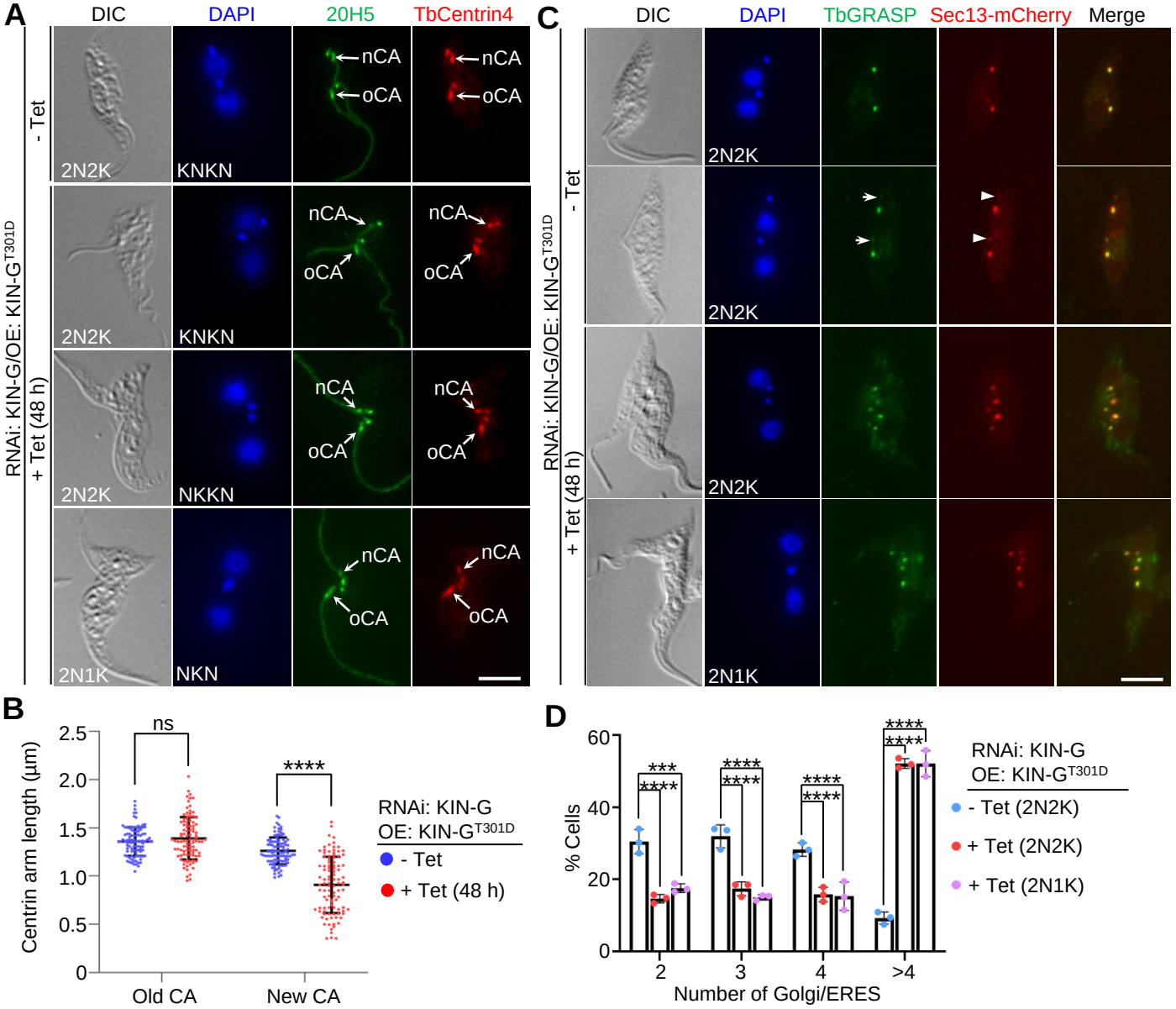
A
DIC
DAPI
20H5
TbCentrin4
RNAi: KIN-G/OE: KIN-G^{T301D}
- Tet
+ Tet (48 h)
2N2K
KNKN
nCA
oCA
2N2K
KNKN
2N2K
NKKN
2N1K
NKN
B
Centrin arm length (µm)
ns
****
Old CA
New CA
RNAi: KIN-G
OE: KIN-G^{T301D}
- Tet
+ Tet (48 h)
C
DIC
DAPI
TbGRASP
Sec13-mCherry
Merge
2N2K
2N1K
D
% Cells
***
****
Number of Golgi/ERES
2
3
4
>4
RNAi: KIN-G
OE: KIN-G^{T301D}
- Tet (2N2K)
+ Tet (2N2K)
+ Tet (2N1K)

Figure 6

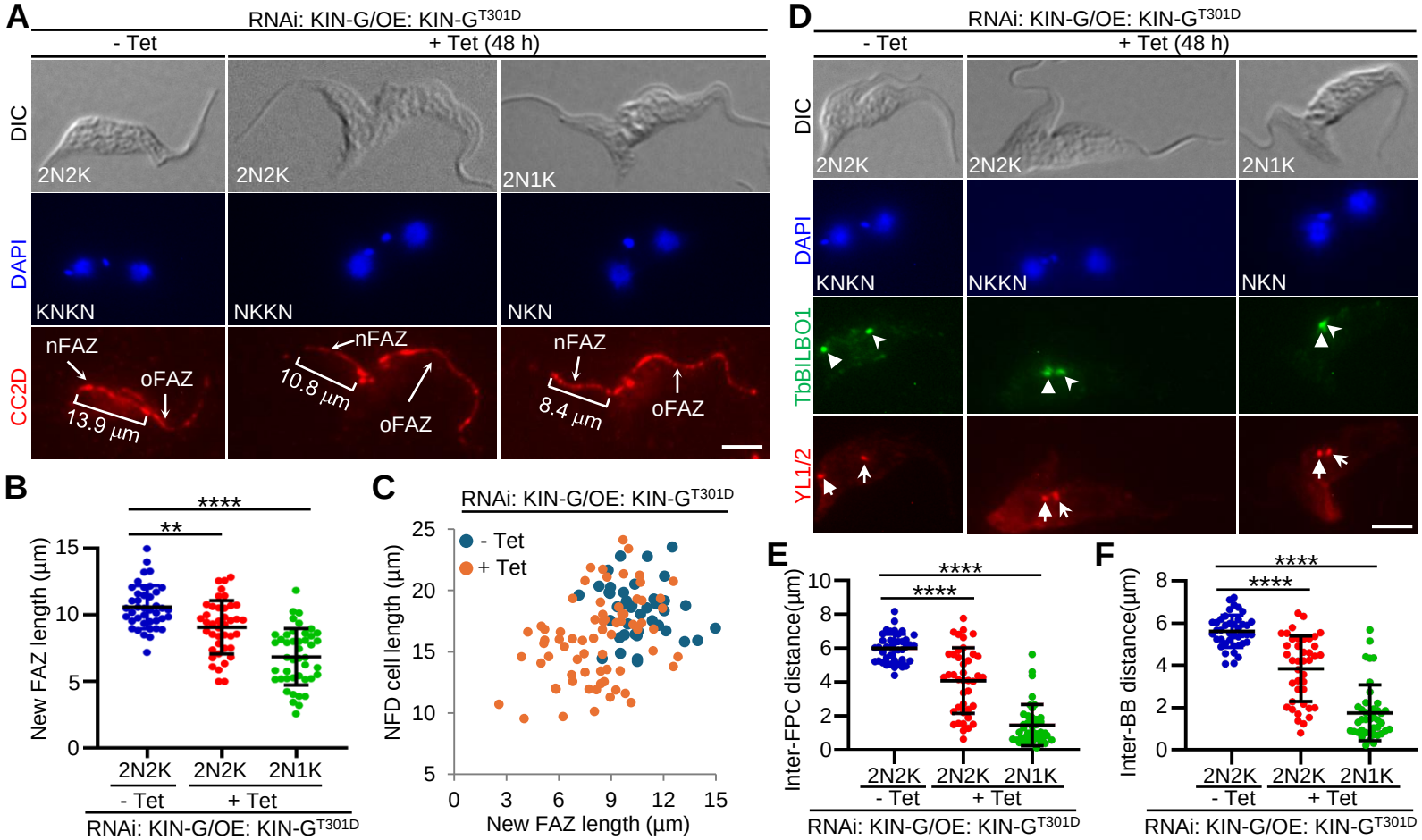
A
RNAi: KIN-G/OE: KIN-G^{T301D}
- Tet
+ Tet (48 h)
DIC
DAPI
CC2D
2N2K
2N2K
2N1K
KNKN
NKKN
NKN
nFAZ
oFAZ
13.9 µm
10.8 µm
8.4 µm
B
New FAZ length (µm)
****
**
2N2K
2N2K
2N1K
- Tet
+ Tet
RNAi: KIN-G/OE: KIN-G^{T301D}
C
RNAi: KIN-G/OE: KIN-G^{T301D}
- Tet
+ Tet
NFD cell length (µm)
New FAZ length (µm)
D
RNAi: KIN-G/OE: KIN-G^{T301D}
- Tet
+ Tet (48 h)
DIC
DAPI
TbBILBO1
YL1/2
2N2K
2N2K
2N1K
KNKN
NKKN
NKN
E
Inter-FPC distance(µm)
****
****
2N2K
2N2K
2N1K
- Tet
+ Tet
RNAi: KIN-G/OE: KIN-G^{T301D}
F
Inter-BB distance(µm)
****
****
2N2K
2N2K
2N1K
- Tet
+ Tet
RNAi: KIN-G/OE: KIN-G^{T301D}

Figure 7

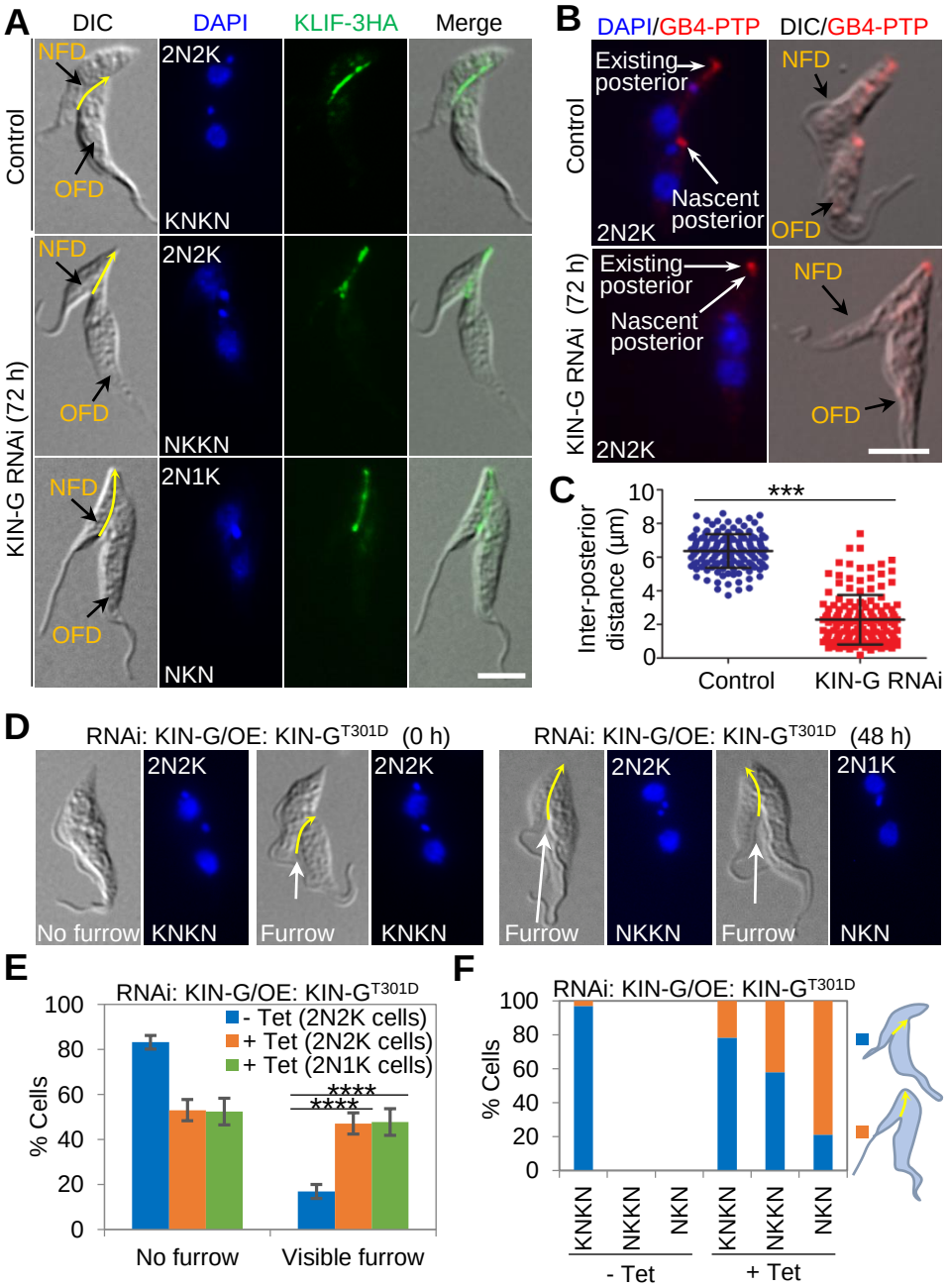
A
DIC
DAPI
KLIF-3HA
Merge
Control
KIN-G RNAi (72 h)
NFD
OFD
2N2K
KNKN
NKKN
2N1K
NKN
B
DAPI/GB4-PTP
DIC/GB4-PTP
Existing posterior
Nascent posterior
2N2K
C
Inter-posterior distance (µm)
***
Control
KIN-G RNAi
D
RNAi: KIN-G/OE: KIN-G^{T301D} (0 h)
RNAi: KIN-G/OE: KIN-G^{T301D} (48 h)
No furrow
Furrow
E
RNAi: KIN-G/OE: KIN-G^{T301D}
- Tet (2N2K cells)
+ Tet (2N2K cells)
+ Tet (2N1K cells)
% Cells
****
No furrow
Visible furrow
F
RNAi: KIN-G/OE: KIN-G^{T301D}
% Cells
- Tet
+ Tet